The characterization of telephone cord buckling of compressed thin films on substrates

M.W. Moon[a,d,*], H.M. Jensen[b], J.W. Hutchinson[c], K.H. Oh[a], A.G. Evans[d]

[a] *School of Material Science and Engineering, Seoul National University, San-56-1, Sillim-Dong, Kwanak-Gu, Seoul 151-744, South Korea*
[b] *Department of Solid Mechanics, Technical University of Denmark, Lyngby, DK-2800, Denmark*
[c] *Division of Engineering and Applied Sciences, Harvard University, Cambridge, MA 02138, USA*
[d] *Princeton Materials Institute, Princeton University, NJ 08540, USA*

Abstract

The topology of the telephone cord buckling of compressed diamond-like carbon films (DLC) on glass substrates has been characterized with atomic force microscopy (AFM) and with the focused ion beam (FIB) imaging system. The profiles of the several buckles have been measured by AFM to establish the symmetry of each repeat unit, revealing similarity with a circular buckle pinned at its center. By making parallel cuts through the buckle in small, defined locations, straight-sided buckles have been created on the identical films, enabling the residual stress in the film to be determined from the profile.

It has been shown that the telephone cord topology can be effectively modeled as a series of pinned circular buckles along its length, with an unpinned circular buckle at its front. The unit segment comprises a section of a full circular buckle, pinned to the substrate at its center. The model is validated by comparing radial profiles measured for the telephone cord with those calculated for the pinned buckle, upon using the residual stress in the film, determined as above. Once validated, the model has been used to determine the energy release rate and mode mixity, $G(\psi)$.

The results for $G(\psi)$ indicate that the telephone cord configuration is preferred when the residual stress in the DLC is large, consistent with observations that straight-sided buckles are rarely observed, and, when they occur, are generally narrower than telephone cords. Telephone cords are observed in many systems, and can be regarded as the generic morphology. Nevertheless, they exist subject to a limited set of conditions, residing within the margin between complete adherence and complete delamination, provided that the interface has a mode II toughness low

---

* Corresponding author. School of Material Science and Engineering, Seoul National University, San-56-1, Sillim-Dong, Kwanak-Gu, Seoul 151-744, South Korea. Tel.: +82-2-872-83-7.

E-mail address: mwmoon@snu.ac.kr (M.W. Moon).

enough to ensure that the buckle crack does not kink into the substrate. © 2002 Elsevier Science Ltd. All rights reserved.

Keywords: A. Buckling; Fracture toughness; B. Coatings; Films; C: Stability and Bifurcationn

1. Introduction

Residually compressed thin films on thick substrates may buckle. The buckles propagate beneath the film if the induced energy release rate exceeds the interface fracture toughness. The associated mechanics has been documented (Evans and Hutchinson, 1984; Hutchinson et al., 1992; Hutchinson and Suo, 1992; Thouless et al., 1992; Jensen and Thouless, 1995; Evans et al., 1997; Chai, 1998; Hutchinson et al., 2000; Audoly, 2000; Hutchinson, 2001). The buckles exhibit several configurations: ranging from circular, to linear to telephone cord (Fig. 1) (Matuda et al., 1981; Gille and Rau, 1984; Lee et al., 1993; Colin et al., 2000; Moon et al., 2002). *Straight buckles* propagate with a curved front. The conditions at the stationary side and the circular front have been
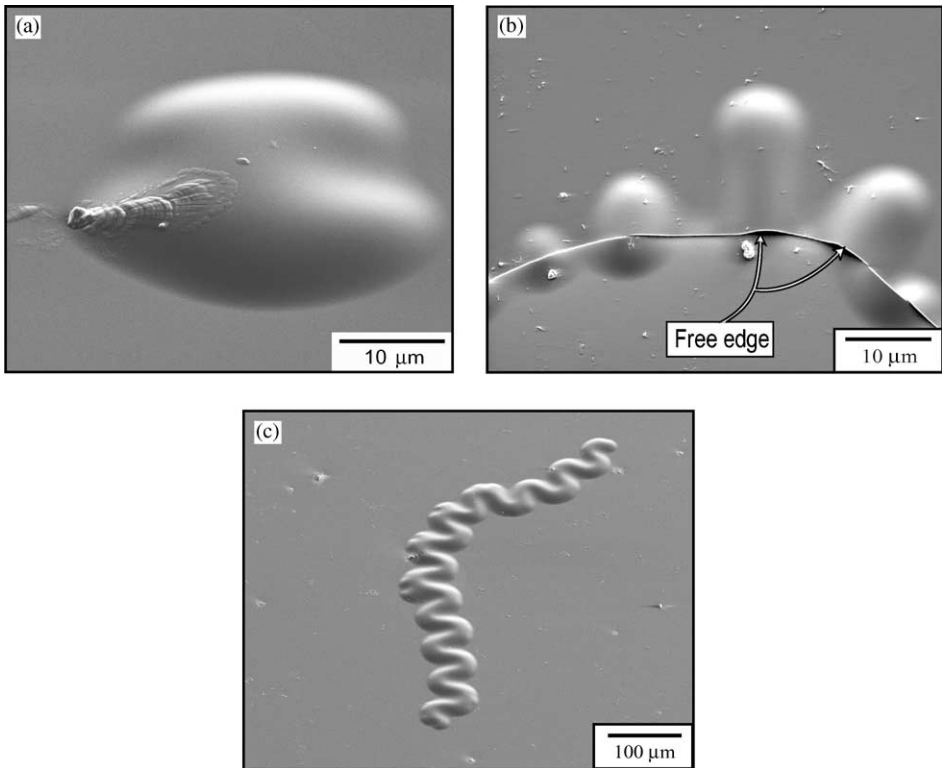

Fig. 1. Illustrations of straight-sided, circular, and telephone cord buckles (Moon et al., 2002).

modeled and rationalized in terms of mode mixity and energy release rate (Hutchinson and Suo, 1992; Hutchinson, 2001; Jensen and Sheinman, 2001). The corresponding mechanics for *telephone cord buckles* are less well developed. The purpose of this study is to gain some insight by performing measurements on thin films of diamond-like carbon (DLC) deposited onto nominally flat glass substrates and conducting a corresponding mechanics assessment. Such systems are typically subject to high residual compression (1–4 GPa) and modest adhesion, causing them to be susceptible to telephone cord buckles.

The profiles of telephone cord buckles are characterized along different chords, by using the atomic force microscope (AFM). To make a direct comparison between telephone cord and (the more completely understood) straight-sided buckles, the focused ion beam (FIB) imaging system has been used to create two parallel (damage free) cuts, converting a section of the former into the latter. Changes in the profile before and after cutting can be used to correlate the two configurations, with all other variables fixed. The ensuing measurements provide a direct assessment of the mechanics of telephone cord buckling.

2. Measurements

2.1. Procedures

Diamond-like carbon films were deposited on glass microscope slides by using a capacitively coupled glow discharge of CH_4 and C_6H_6 plus N_2, at a deposition pressure of 1.33 Pa, with negative self-bias voltage controlled in the range from -100 to -700 V by adjusting the r.f. power (Cho et al., 1999). For these conditions, the film thickness is in the range, 0.13–0.47 μm, and the residual compression between 1 and 3 GPa, resulting in telephone cord buckles with a wide range of wavelengths between 1.5 and 25 μm.

Images of representative buckles have been obtained by using the AFM in tapping mode (Digital Instrument company) while also obtaining information about their profiles. Sections through the buckle were made by using the Dual-Beam FIB (FEI Company, DB235). The change in profile caused by cutting was determined with the AFM. Multiple sections were cut and analyzed in the same manner.

2.2. Buckling profiles

Images of the telephone cord buckles (Fig. 2) suggest that each repeated unit has a center of symmetry, denoted O in the figure, and that the circumference around that point, denoted by the arc XY, has constant curvature. The adjacent units have the inverse symmetry. Each repeated unit occupies roughly a $90°$ angular domain.

AFM profiles measured along representative trajectories for a DLC film (thickness, $h = 0.13$ μm) affirm the overall characteristics (Figs. 3 and 4). All the *radial trajectories* originating at O have essentially the same asymmetric profile, exemplified by that shown in Figs. 3a, b. Note the small deviations from constancy within the four radial
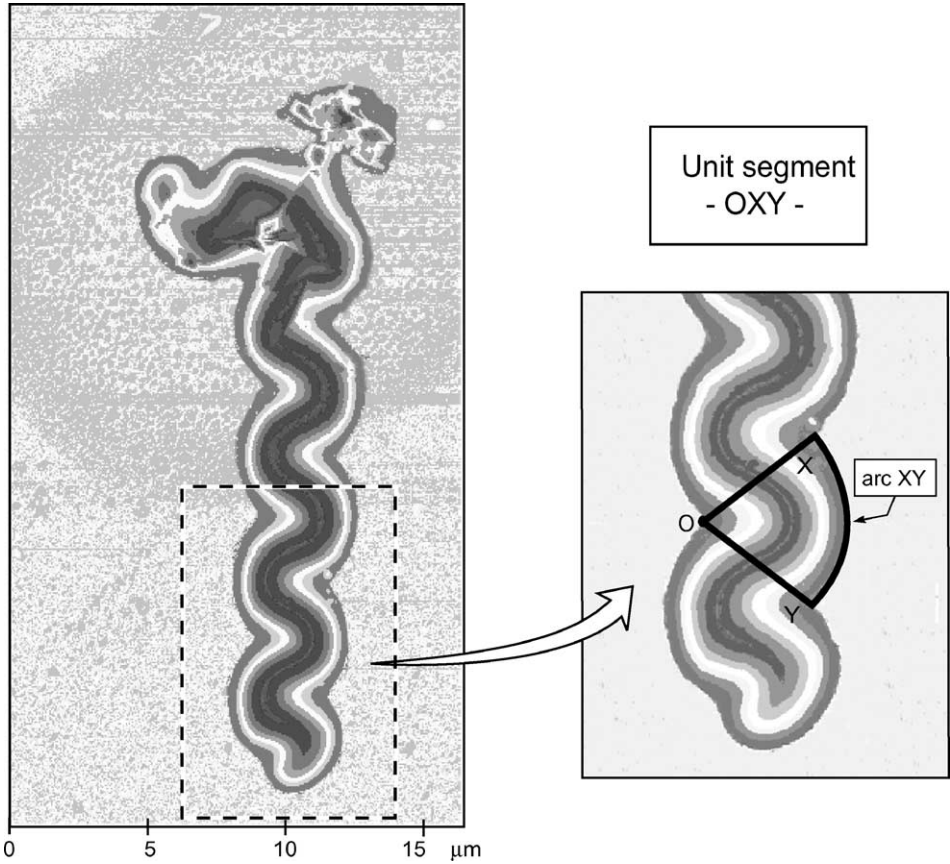
Fig. 2. Plan view of a telephone cord buckle, used to highlight a unit segment with center of curvature at O and arc length XY.

trajectories, $\bar{C}, \bar{C}_1, \bar{C}_2, \bar{C}_3$, as well as the mirror symmetry between $\bar{A}(\bar{E})$ and $\bar{C}$. Profiles along the medians between adjacent units [lines $\bar{B}(\bar{D})$ on Fig. 3a] are symmetric (Fig. 3c). The wavelengths b_1, b_2 and b_3 measured for films with a range of thickness (Fig. 5) reveal *a linear dependence on h*. Moreover, the ratio of wavelengths, b_i/b_1 ($i=2,3$), is essential invariant with film thickness, expressing the self-similarity of the buckle profiles.

Profiles at the front, along lines $\bar{F}$ ($\bar{F}_1$ and $\bar{F}_2$) on Fig. 3a, are compared with those along the center of the unit segment, $\bar{C}$, on Fig. 3d. Note that the peak amplitude diminishes as the tip is approached and that the profile becomes more symmetric.

2.3. Sectional profiles

The effects of FIB cutting straight-sided sections from the telephone cord are visualized in Fig. 6. Measurements of profiles before and after cutting are presented in
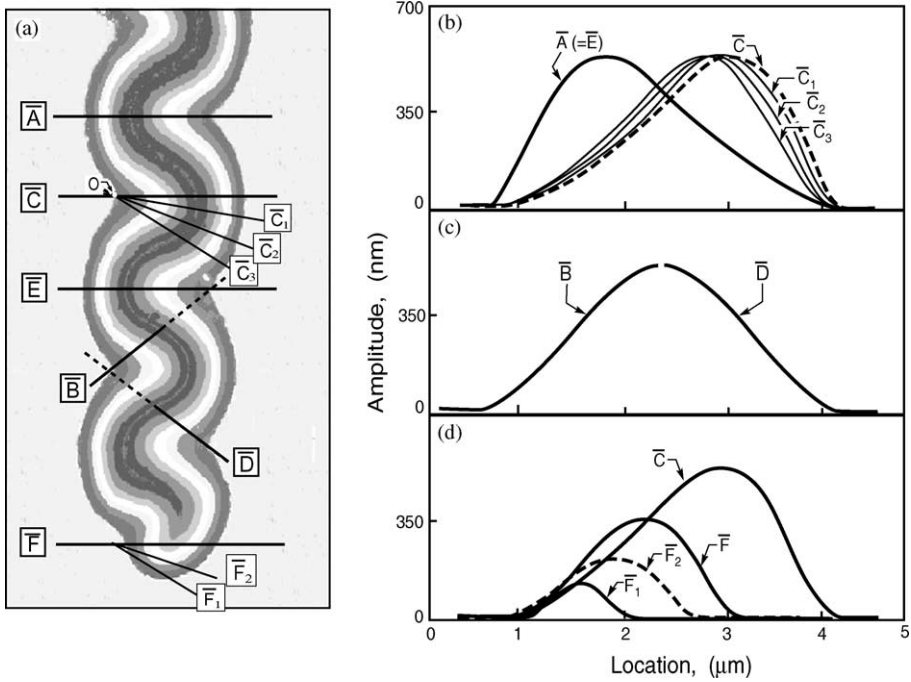
Fig. 3. (a) Image of a telephone cord buckle indicating the radial trajectories used for profile characterization (C, A and E), as well as the medians (B and D), and locations at the front (F). (b) The profiles along the radial trajectories, obtained using the AFM. Note that the trajectories $\bar{A}$ and $\bar{E}$ lie on top of each other. (c) The profile along the medians. (d) The profiles measured near the front compared with a radial profile.

Fig. 7 (thickness, $h = 0.47\,\mu\text{m}$). The two sections closest to the center (B and C) reveal that the initial asymmetric profiles become symmetric with essentially the same overall wavelength (58 and 58 µm, respectively), Table 1. That is, *the buckles do not extend laterally when sectioned*. This finding has implications for the energy release rate, elaborated below. The sections at the sides (A and D) become more symmetric, but there are "tails" (arrowed) at one side, suggestive of contact between the film and substrate within the buckle.

3. Associated mechanics

3.1. Straight-sided buckles

For thin films, thickness h, subject to equi-biaxial compression, σ_0, the surface displacement w normal to the substrate of a *straight sided buckle* (Figs. 8a, b), as a function of distance y measured from the middle of the buckle well behind the curved
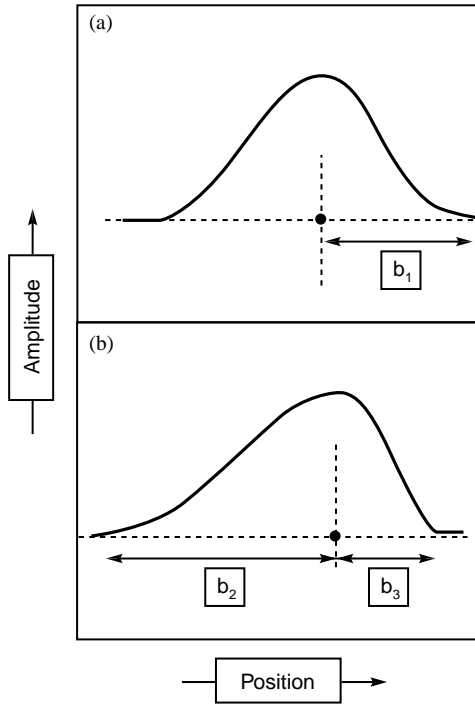
Fig. 4. Schematics of symmetric and asymmetric profiles defining the wavelengths: (a) the symmetric medians (*B* and *D*) and (b) the asymmetric radial profile (*C*).

front, is given by (Hutchinson and Suo, 1992)

$$\frac{w}{h} = \frac{\xi}{2}(1 + \cos(\pi y/b)), \tag{1}$$

where $2b$ is the width and

$$\xi \equiv \frac{w_{\max}}{h} = \sqrt{\frac{4}{3}\left(\frac{\sigma_0}{\sigma_c} - 1\right)}. \tag{2}$$

The critical bifurcation stress, σ_c, at width $2b$, is

$$\sigma_c = \left(\frac{\pi^2}{12}\right)\frac{E}{1 - v^2}\left(\frac{h}{b}\right)^2 \tag{3}$$

with E and v being Young's modulus and Poisson's ratio of the film, respectively. The energy release rate and phase angle, $\tan\psi_s \equiv K_{II}/K_I$, *on the sides*, well behind the
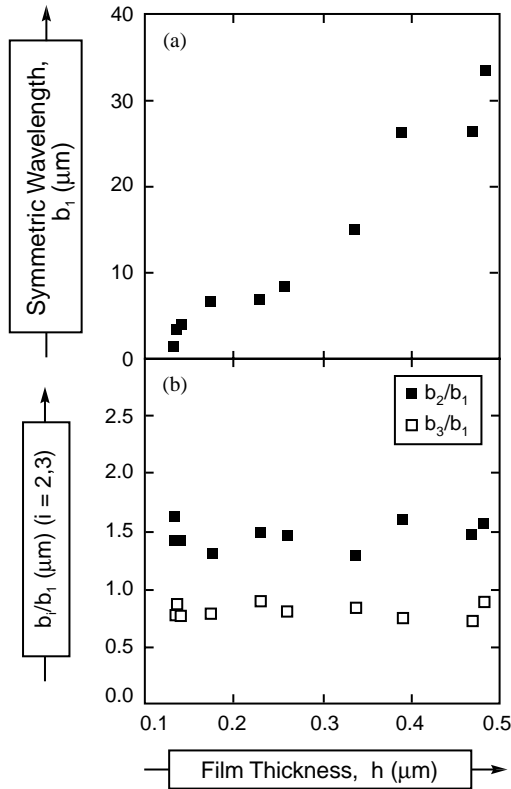
Fig. 5. Experimental measurements of the wavelength b_1, b_2 and b_3 for a range of film thickness. (a) The wavelength obtained on symmetric sections increases proportionally with thickness of film. (b) The ratios of the asymmetric to symmetric wavelengths, b_i/b_1 $(i = 2, 3)$ are invariant with film thickness.

curved front, are:

$$G_s/G_0 = \left(1 - \frac{\sigma_c}{\sigma_0}\right)\left(1 + 3\frac{\sigma_c}{\sigma_0}\right),\tag{4}$$

$$\tan\psi_s = \frac{4\cos\omega + \sqrt{3}\xi\sin\omega}{-4\sin\omega + \sqrt{3}\xi\cos\omega},\tag{5}$$

where the energy release rate has been normalized by the strain energy per unit area when the film is released in plane strain (Hutchinson and Suo, 1992):

$$G_0 = (1 - v^2)h\sigma_0^2/2E.\tag{6}$$

Note that the normalized energy release rate, G/G_0, and the maximum deflection, w_{max}/h, depend only on the normalized stress, σ_0/σ_c. The phase angle, ψ, while also a function of the Dundurs' parameters (Hutchinson and Suo, 1992; Suo and Hutchinson,
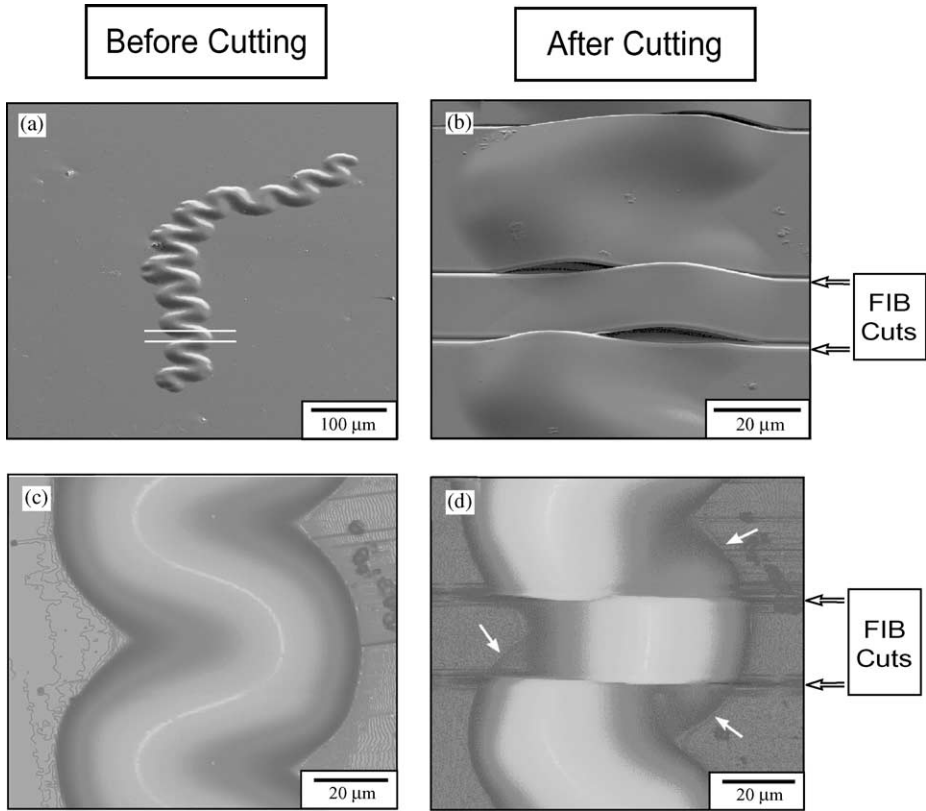
Fig. 6. Images of the cuts produced with the FIB. Note the change of buckle geometry and the discontinuity.

1990), for present purposes is set to the value absent elastic mismatch, whereupon $\omega = 52.1°$. The energy release rate and phase angle along the sides of the straight-sided buckle are plotted on Figs. 9 and 10, respectively.

The steady-state energy release rate averaged over *the curved front* is (Hutchinson and Suo, 1992)

$$G_{ss}/G_0 = (1 - \sigma_c/\sigma_0)^2. \tag{7}$$

The energy release rate along the sides exceeds that along the front at all σ_0/σ_c (Hutchinson, 2001). Yet, the front propagates because it experiences a significant opening mode, while the sides become exclusively mode II, once the buckle attains a characteristic width (associated with $\sigma_0/\sigma_c = 7.54$). Full details will be presented below.

3.2. The sides of telephone cord buckles

Given the symmetry of each unit of the telephone cord buckle, described above (Figs. 2 and 3), it is assumed that the energy release rate and the profile can be *modeled*
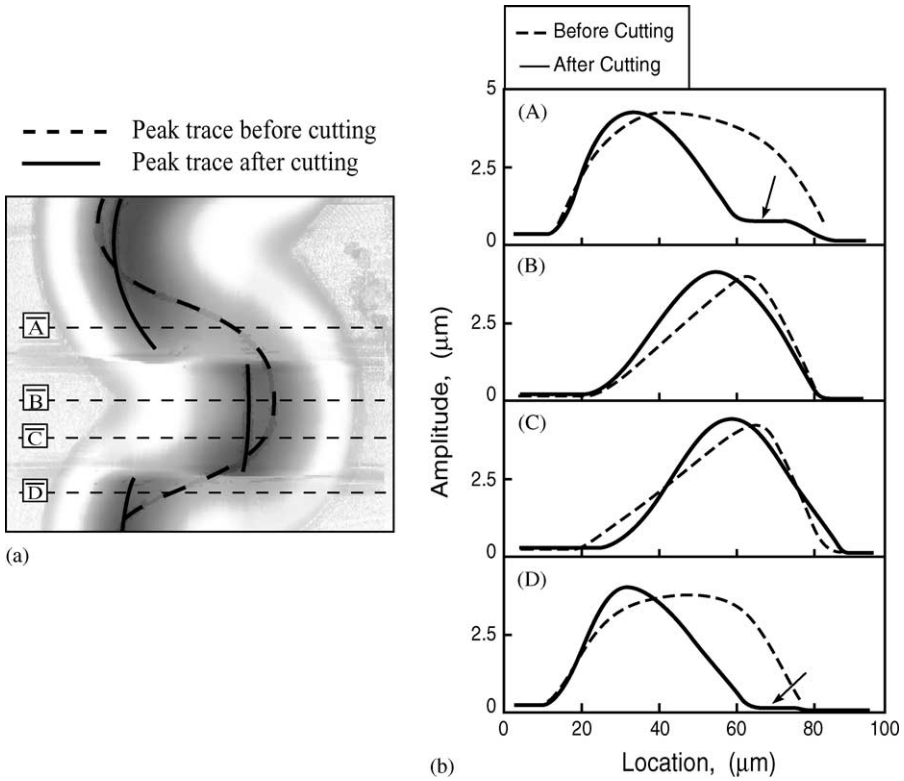
Fig. 7. A comparison of profiles of buckles before and after cutting.

as a full circular buckle, radius $r = R \equiv 2b$, with pinned center (Figs. 8c, d). This assumption is validated below by using the measurements and analysis conducted for the straight-sided buckle created by the FIB. For a circular plate of radius $2b$ pinned to the substrate at the center, the corresponding critical stress is (Evans and Hutchinson, 1984) $\sigma^* = 1.081\sigma_c$, and therefore only slightly greater than that of the straight-sided buckle, width $2b$.

Solutions for the circular, pinned buckle are obtained by numerical integration of the non-linear, axi-symmetric von Karman equations. The equations are written using non-dimensional quantities ($\sim$) upon introducing:

$$\tilde{r} = \frac{r}{R}, \quad \tilde{w} = \sqrt{6(1-v^2)}(w/h), \quad \tilde{\sigma} = 12(1-v^2)\frac{\sigma_0 R^2}{Eh^2},$$

$$\tilde{N} = 12(1-v^2)\frac{NR^2}{Eh^3}. \tag{8}$$

The normal deflection is denoted as w, and N is the radial membrane force in the plate.

Table 1
The profiles before and after cutting: Amplitudes and wavelengths (thickness, $h = 0.47$ μm)

	W_{max} (μm)	b_2 (μm)	b_3 (μm)	$R(=b_2 + b_{34})$ (μm)
Before cutting	3.6–3.8	40	18	58
After cutting	4.0–4.1	29	29	58

The two coupled non-linear plate equations are given by

$$\frac{d}{d\tilde{r}}\left(\frac{d}{d\tilde{r}}\left(\tilde{r}\frac{d^2\tilde{w}}{d\tilde{r}^2}\right) - \frac{d\tilde{w}}{d\tilde{r}}\left(\tilde{r}\tilde{N} + \frac{1}{\tilde{r}}\right)\right) = \tilde{p}\tilde{r},$$

$$\frac{d}{d\tilde{r}}\left(\tilde{r}^3\frac{d\tilde{N}}{d\tilde{r}}\right) + \tilde{r}\left(\frac{d\tilde{w}}{d\tilde{r}}\right)^2 = 0. \tag{9}$$

Here, $\tilde{p}$ is a normal pressure imposed to initially lift the delaminated region from the substrate, chosen to be sufficiently small as not to affect the accuracy of the numerical solution for the residual stresses of interest.

The edges of the delaminated region are taken to be fully clamped to the substrate both at the exterior ($\tilde{r} = 1$) and interior ($\tilde{r} = 1/20$) crack front:

$$w = 0, \quad \frac{dw}{dr} = 0, \quad \frac{d}{d\tilde{r}}(\tilde{r}\tilde{N}) - v\tilde{N} + (1 - v)\tilde{\sigma} = 0. \tag{10}$$

A finite radius of the interior crack front has been taken, $\tilde{r} = 1/20$, sufficiently small as not to influence the results at the exterior front, but sufficiently large to ensure numerical stability, consistent with Fig. 6. The plate equations are integrated numerically in a number of increments, as the residual stress is gradually increased. Equilibrium iterations are performed in each increment to ensure that Eq. (9) is satisfied to a high degree of accuracy.

The energy release rate and the phase angle are calculated using:

$$G = \frac{1 - v^2}{2Eh^3}(12M^2 + h^2(N + \sigma_0 h)^2) \tag{11}$$

and

$$\tan\psi = \frac{K_{II}}{K_I} = \frac{\sqrt{12}M\cos\omega + h(N + \sigma_0 h)\sin\omega}{-\sqrt{12}M\sin\omega + h(N + \sigma_0 h)\cos\omega}, \tag{12}$$

where the bending moment is $M = [Eh^3/(12(1 - v^2))]\,d^2w/dr^2$.

3.3. Comparison of three buckles

Computed results for G/G_0 and ψ for the pinned circular buckle used to model the sides of the telephone cord are presented in Figs. 9 and 10 as a function of σ_0/σ_c. The buckling stress, σ_c, for the straight sided buckle, width $2b$, defined in Eq. (3) is used throughout to normalize the stresses. Included in Figs. 9 and 10 are
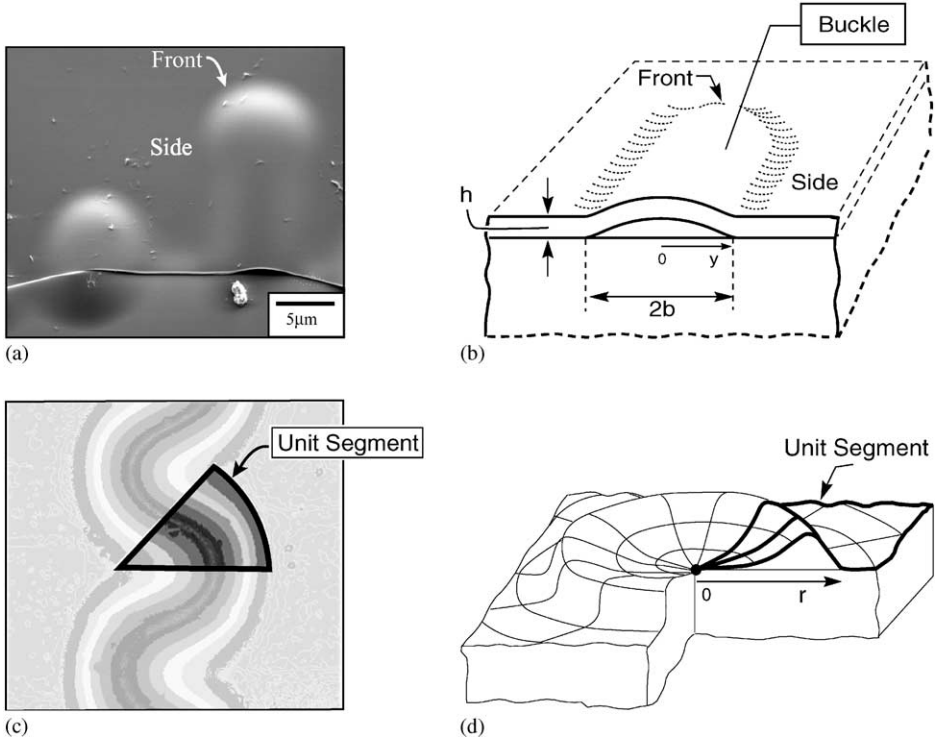
Fig. 8. (a) Images of a short straight-sided buckle and circular buckle. (b) The geometry used for analysis. (c) A unit segment of a telephone cord buckle and (d) the geometry used for analysis.

the corresponding results for an unpinned circular buckle, radius b, obtained by numerical analysis (Hutchinson et al., 1992; Hutchinson and Suo, 1992). The buckling stress is $1.488\sigma_c$. To understand the trends at large σ_0/σ_c in Fig. 9, it is useful to identify the *total elastic energy per unit area* stored in the biaxially stressed film:

$$G_0^* = (1 - v)h\sigma_0^2/E. \tag{13}$$

Note that $G_0^*/G_0 = 1.54$ for a film with $v = 0.3$. As σ_0/σ_c becomes large, equivalent to a large diameter buckle, the energy release rate slowly approaches G_0^*, asymptotically releasing all the stored energy in the film. The corresponding limit for the straight-sided buckle approaches G_0 because the released film remains subject to plane strain constraint parallel to the sides. For further assessment, it becomes convenient to express σ_0/σ_c in terms of the buckle size, b. For this purpose, a reference length is defined as the half-width of the straight-sided configuration at the onset of buckling,

$$b_0 \equiv (\pi/\sqrt{12(1 - v^2)})h\sqrt{E/\sigma_0}, \tag{14}$$

whereupon

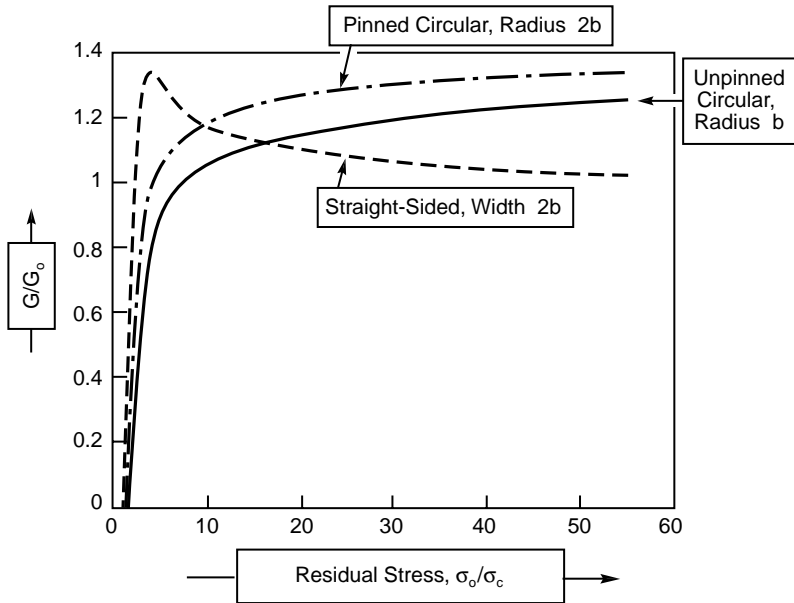$$b/b_0 = \sqrt{\sigma_0/\sigma_c}. \tag{15}$$

Fig. 9. The energy release rates for the three buckles.

The energy release rates for the straight-sided, pinned and circular buckles, summarized on Fig. 9, indicate that G and ψ for the circular buckle and at the sides of the telephone cord are similar. By comparison, G at the sides of the straight buckle is smaller, at least when the stress is large, $\sigma_0/\sigma_c \geqslant 9$ (as in the present case, addressed below). Moreover, when $\sigma_0/\sigma_c \geqslant 7.5$, the sides of the straight buckle experience pure mode II, while the circular buckles retain a substantial component of mode I.

The normal deflections for the straight-sided and pinned buckles calculated at three levels of residual stress are compared in Fig. 11. Note the asymmetry of the pinned configuration, which increases as the stress increases. The peak displacement for the pinned configuration is a little lower than that of straight-sided configuration.

4. Analysis of the telephone cord morphology

The existence of the telephone cord morphology is intimately related to interfaces having toughness that increases with increasing proportion of mode II to mode I. Indeed, as revealed in earlier work (Hutchinson et al., 1992; Hutchinson and Suo, 1992; Hutchinson, 2001), the occurrence of stable propagation owes its existence to this mode dependence. The tendency to develop a curved delamination front is tied to the larger proportion of mode I relative to mode II as the buckle enlarges. The proclivity for mode II behavior along straight edges is evident from Fig. 10.

To simulate features of telephone cords with the solutions for circular and pinned circular buckles, it is useful to introduce a phenomenological representation of a family
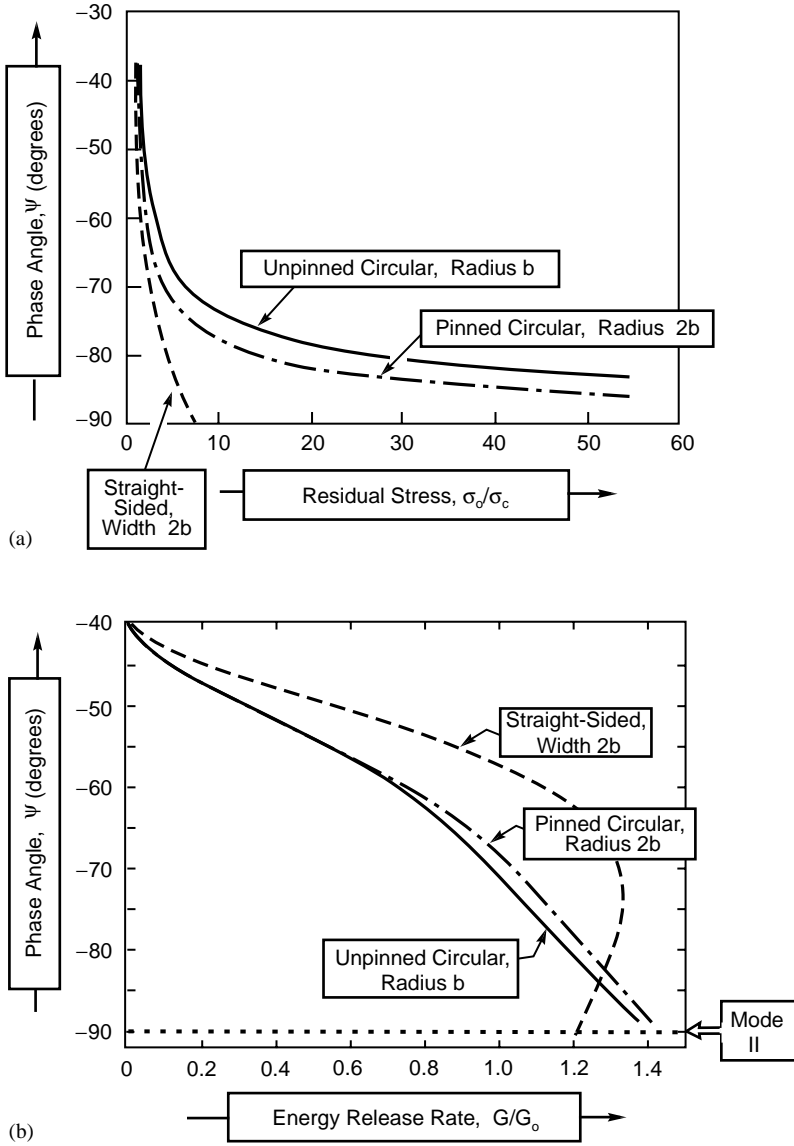
Fig. 10. The mode mixity for the three different buckles: (a) dependence on the stress and (b) dependence on energy release rate.

of interface toughness dependencies (Hutchinson and Suo, 1992)

$$\Gamma_c(\psi) = \Gamma_{lc} f(\psi),$$

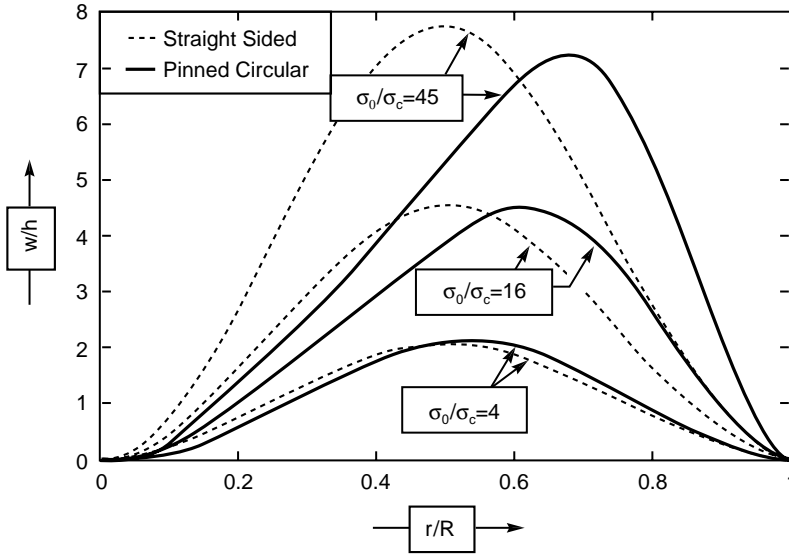$$f(\psi) = (1 + \tan^2((1 - \lambda)\psi)), \tag{16}$$

Fig. 11. The normal deflection for straight-sided buckles (broken lines) and pinned, axi-symmetric buckles (solid lines).

where $\Gamma_c(\psi)$ is the mode-dependent interface toughness, Γ_{Ic} the mode I toughness and λ is a mode-sensitivity parameter that sets the strength of the mode dependence (Fig. 12). The criterion for propagation of a crack in the interface is $G = \Gamma_c(\psi)$. The ratio of mode II to mode I toughness of the interface is $\Gamma_{IIc}/\Gamma_{Ic} = 1 + \tan^2((1-\lambda)\pi/2)$. Interfaces with moderately strong dependence typically have $\lambda < 0.3$ (Evans et al., 1990).

A mode-adjusted energy release rate, F, provides insight into the tendency of buckles to propagate on curved rather than straight edges (Hutchinson, 2001). With $\Gamma_c(\psi) = \Gamma_{Ic} f(\psi)$, let

$$F \equiv G/f(\psi), \tag{17}$$

such that the criterion for propagation of the interface crack becomes $F = \Gamma_c$. The trends (Fig. 13) have been determined from the results for G/G_0 and ψ in Figs. 9 and 10, upon using (16) with $\lambda = 0.25$. Note that, when σ_0/σ_c exceeds about 3 (or, equivalently, when $b/b_0 > \sqrt{3}$), the mode adjusted energy release rate on the straight edge is lower than that on curved sides. This behavior underlies the tendency of highly stressed films to display curved buckle morphologies. It also explains why a straight-sided buckle propagates at its curved front rather than spreads from its straight sides.

The stabilization of the sides of telephone cords and their dimensions can be addressed by imposing $G = \Gamma_c(\psi)$ (equivalently, $F = \Gamma_c$) on the solution for the pinned circular buckle, upon using the results from Figs. 9 and 10 and the interface toughness function (16). The results yield the total elastic energy $G_0^* = (1 - \nu)h\sigma_0^2/E$, needed to satisfy the fracture criterion. The energy is normalized by the mode II toughness (Fig. 14), motivated by the knowledge that as the buckle becomes large it approaches mode
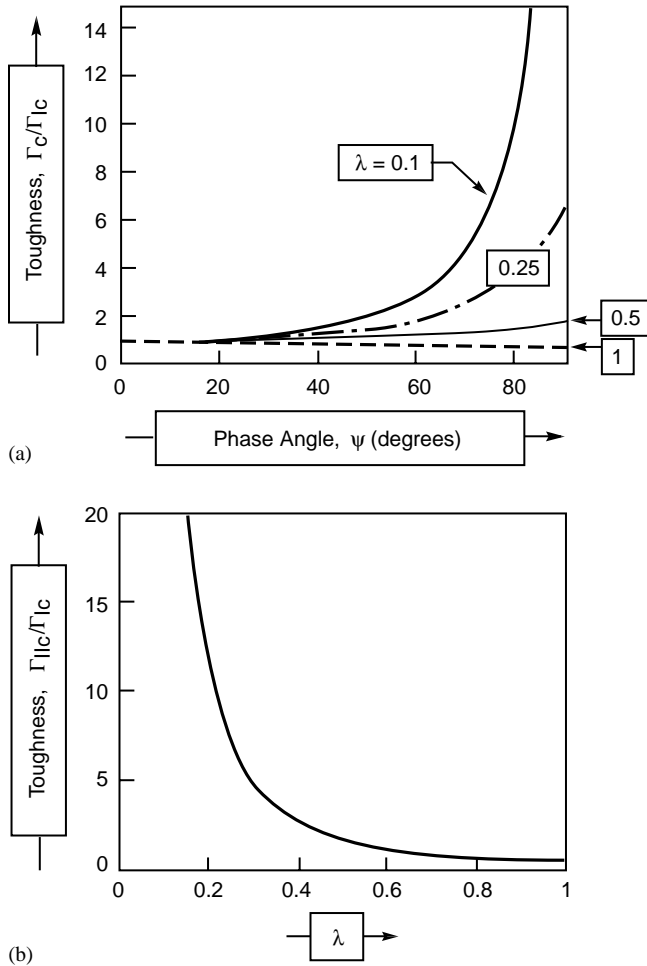
Fig. 12. (a) The toughness as a function of mixity for several choices of the mode sensitivity parameter, λ. (b) The ratio of the mode II toughness to that in mode I for the full range of the mode sensitivity parameter, λ.

II. Note that, if the Griffith criterion ($\lambda = 1$) were in effect, the energy G_0^* needed to propagate the interface crack would *diminish* as b increases: whereupon, once initiated, the interface crack would delaminate the film dynamically. Stabilization requires *increasing* G_0^* with increasing b. This occurs when $\lambda < 0.5$ ($\Gamma_{\mathrm{IIc}}/\Gamma_{\mathrm{Ic}} > 2$, Fig. 12), once b/b_0 exceeds about 2. To estimate the dimension, $2b$, of the telephone cord from the solution for the pinned circular plate (Fig. 14), it is necessary to know both Γ_{IIc} and λ, in addition to the stress in the film and its thickness. These quantities are assessed in Section 5.

To further illuminate the morphology, curves for $G_0^*/\Gamma_{\mathrm{II}}$ for the pinned circular buckles, radius $2b$, from Fig. 14 are presented in Fig. 15. Corresponding curves are shown
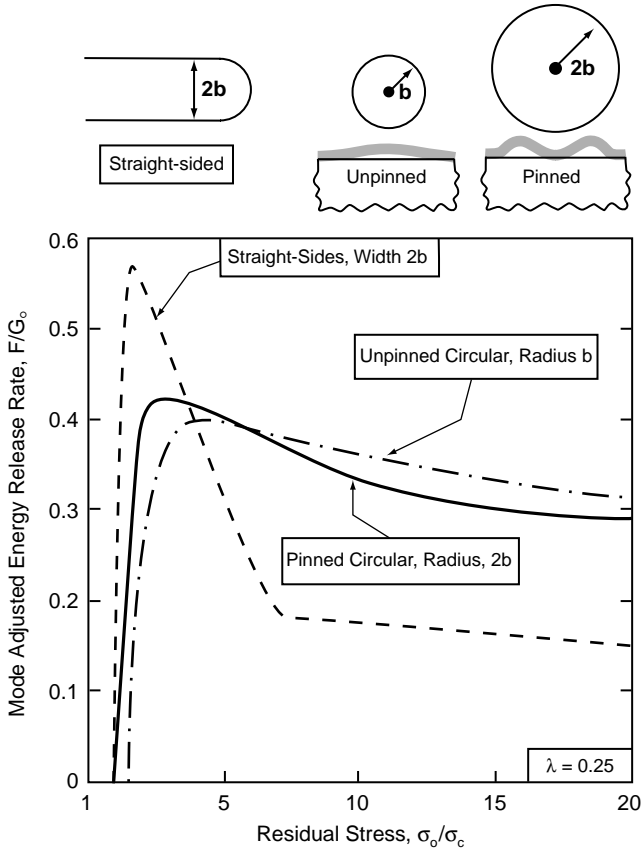
Fig. 13. Mode adjusted energy release rate, F/G_0, for three cases as a function of normalized film stress, $\sigma_0/\sigma_c = (b/b_0)^2$, for the mode dependence in (16) with $\lambda = 0.25$. The result for the straight-sided blister refers to the sides well behind the curved front. The change in slope for the straight-sided blister, at $\sigma_0/\sigma_c \cong 7.5$ occurs at the transition to pure mode II.

for $G_0^*/\Gamma_{\mathrm{II}}$ required to maintain the condition $G/\Gamma_c(\psi)$ at the edge of an unconstrained circular buckle, radius R. The sides of the telephone cord are represented by the edge of the pinned circular buckle, radius $2b$, as already discussed. The energy release rate at the propagating front (see inset in Fig. 15) has been approximated by that for an unconstrained circular buckle, radius $R = b$. The lower energy density, G_0^*, required to extend the front relative to the sides is consistent with the sides remaining stationary.

5. Interpretation of the measurements

The preceding analysis is used in conjunction with the measurements and observations, before and after FIB cutting, in the following manner. (i) The profile of the cut,
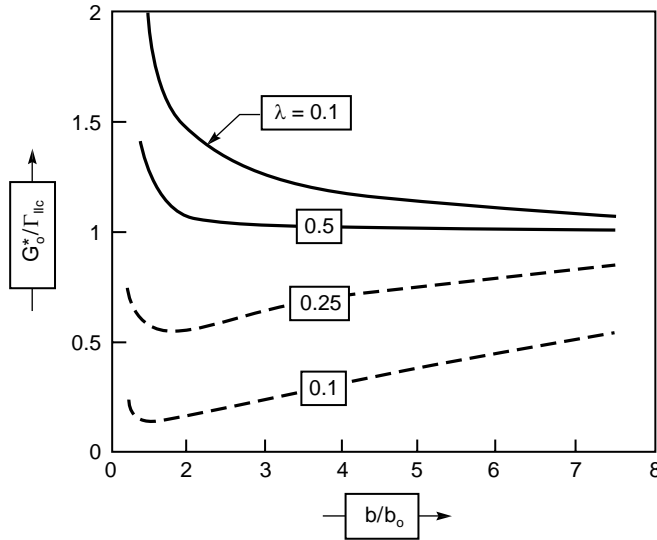
Fig. 14. The ratio of the total strain energy in the film to the mode II interface toughness, as a function of the buckle diameter, $2b$, showing the effect of the mode sensitivity parameter λ on the crack stability. That is, for $\lambda \leqslant 0.5$, the total energy needed to extend the crack increases with increase in b, indicative of stable propagation, in accordance with the experimental findings.

straight-sided buckle is used with Eq. (1) to determine the unknown residual stress in the DLC film, σ_0. (ii) This stress is used with the solution to Eq. (10), as illustrated in Fig. 11, to predict the radial profiles for the unit segment of the telephone cord buckle. (iii) The calculated profiles are compared with the measurements to assess the validity of the pinned, circular buckle assumption. (iv) Once validated, to gain some understanding about buckle formation and propagation, the model is used to calculate energy release rates at the sides of the telephone cord as well as at the front.

Ascertaining the width ($b = 29\,\mu$m) and amplitude ($w_{max}/h = 8.5$) of the straight-sided buckles from Fig. 7 (Table 1), and inserting into the solution for the profile, along with the film thickness ($h = 0.47\,\mu$) and the DLC properties ($E = 120$ GPa, $v = 0.3$ (Cho et al., 1999)), the stress ratio is determined as $\sigma_0/\sigma_c = 55$. Upon using Eq. (3) to obtain σ_c, the residual stress becomes $\sigma_0 = 1.6$ GPa (Cho et al., 1999).

The profiles of pinned buckles are now compared with the radial trajectories measured experimentally (Fig. 7b). The wavelengths indicated in Table 1 ($b_2 + b_3 = 58\,\mu$m), with the residual stress, $\sigma_0/\sigma_c = 55$, predict an amplitude maximum, $w_{max}/h = 7.9$. This amplitude is essentially the same as the measured value (Table 1). The full profiles are compared in Fig. 16. Note the accuracy with which the pinned circular buckle solution captures the radial profiles measured on the telephone cords. The closeness of this comparison validates the use of the pinned, full circular buckle as a model for a unit segment of the telephone cord.

With these stresses and dimensions, the energy release rate at the side of a telephone cord buckle is calculated as $G = 1.34G_0 = 6.1$ J/m^2, primarily in mode II, with a small
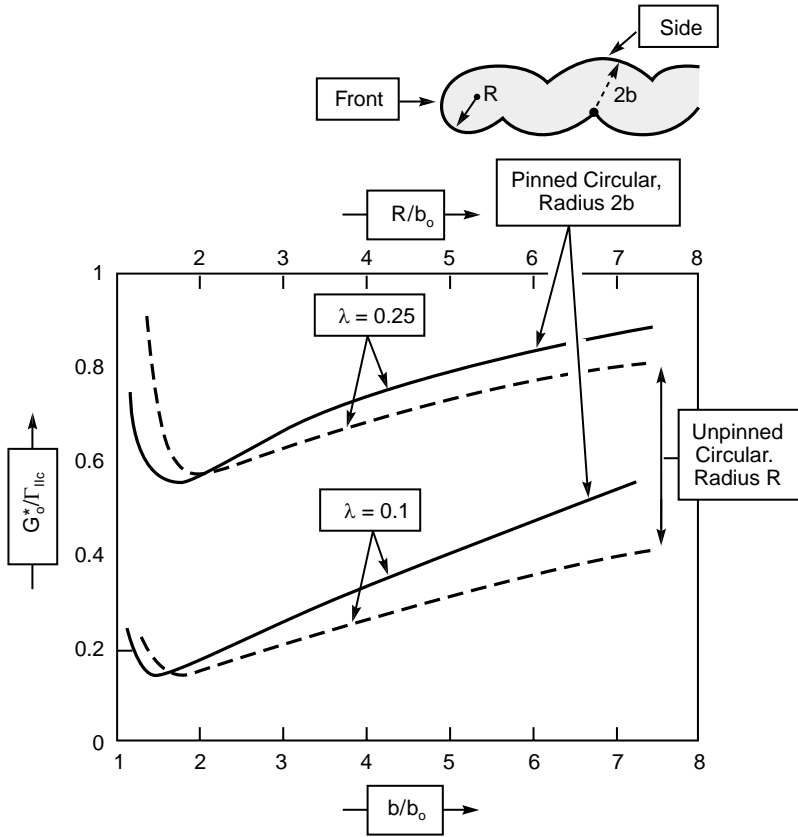
Fig. 15. Comparison of the behaviors at the sides and the front of a telephone cord buckle for small values of the mode sensitivity parameter. The key feature is that, for both λ, less stored energy, G_0^* is needed to extend the buckle at the front than along the sides.

component of mode I (Fig. 10). Note that this G is similar to the interface toughness ascertained in a previous study (Moon et al., 2002). The corresponding energy release rate after cutting, obtained by using the profiles from Fig. 7 ($b = 29$ μm, $w_{max}/h = 8.5$), with the same residual stress ($\sigma/\sigma_c = 55$ (Eq. (3))) is, $G = 1.04G_0 = 4.7$ J/m^2, in pure mode II (Fig. 10). The lower value at comparable mode mixity is consistent with the observation that the buckle does not extend laterally after cutting (Fig. 7). To estimate the energy release rate at front, the solution for a circular buckle has been used (Hutchinson, 2001). The measured frontal radius, $R = 20$ μm, when used with the same residual stress gives $\sigma_0/\sigma_c = 67$, such that, $G = 1.11G_0 = 5.1$ J/m^2. These measurements provide $G_0^* = 7.0$ J m^{-2} and $b/b_0 = \sqrt{\sigma_0/\sigma_c} = 7.4$, enabling the results in Fig. 14 to be used to estimate Γ_{IIc}. For $\lambda = 0.25$, $\Gamma_{IIc} = 8.1$ Jm^{-2} ($\Gamma_{Ic}/\Gamma_{IIc} = 0.146$), while for $\lambda = 0.1$, $\Gamma_{IIc} = 12.2$ Jm^{-2} ($\Gamma_{Ic}/\Gamma_{IIc} = 0.024$). The estimate $\Gamma_{IIc} = 8.1$ Jm^{-2} for $\lambda = 0.25$ is probably the more realistic.
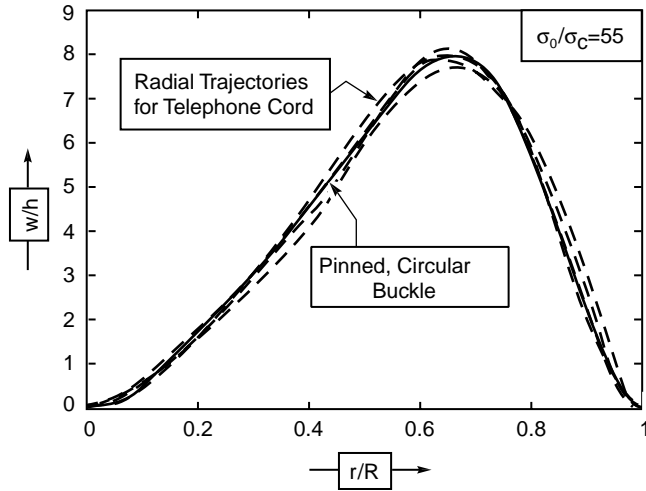
Fig. 16. A comparison of measured and predicted radial profiles for a unit segment of the telephone cord buckle.
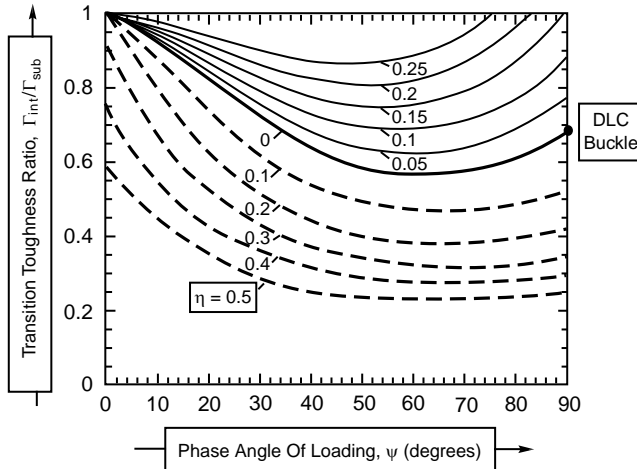

Fig. 17. A plot of the toughness domain wherein an interface crack deviates into the substrate. The quantity η is a non-dimensional measure of the residual stress in the substrate. Here it is taken as zero and the relevant point is indicated as "DLC" buckle.

Finally, note that the energy release rates at the sides and the front are all lower than the mode I toughness of the substrate, $\Gamma_{sub} \approx 8 \text{ J/m}^2$ (Weiderhorn, 1967). The kinking of a crack out of the interface into the substrate would require a larger interface toughness (He and Hutchinson, 1989a, b; He et al., 1991) in accordance with the ratio plotted on Fig. 17 (He et al., 1991). According to this criterion, a mode II
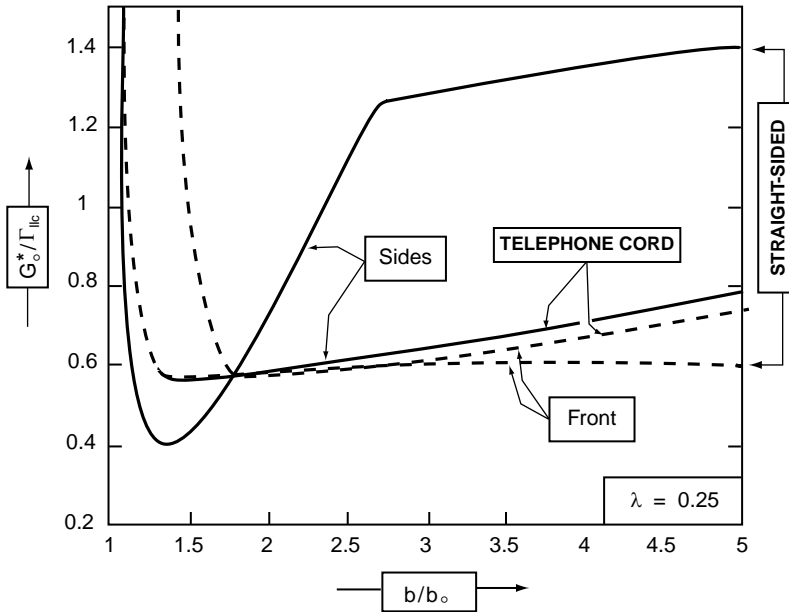
Fig. 18. Competition between telephone cord and straight-sided buckles. Normalized energy per unit area in the film required to propagate the sides and front of both telephone cord and straight-sided buckles as a function of half-width for $\lambda = 0.25$ ($\Gamma_{\mathrm{IIc}}/\Gamma_{\mathrm{Ic}} = 6.8$). Conditions for stability of the straight-sided buckle are limited to $G_0^*/\Gamma_{\mathrm{IIc}} \cong 0.6$ and $b/b_0 \cong 2$.

interface crack would only deviate into the substrate when the interface toughness satisfies $\Gamma_{\mathrm{int}} > 0.78\Gamma_{\mathrm{sub}} \cong 6\,\mathrm{J/m}^2$. This assessment affirms that the buckle is only marginally stable at the interface.

6. Competition between telephone cord and straight-sided morphologies

The preceding analysis and interpretation allow new insights to be gained about the competition between the telephone cord and straight-sided configurations. Based on the energy per area in the film associated with the telephone cord (Fig. 15), together with corresponding results for the straight-sided blister, from (4)–(7), the normalized energy per area, $G_0^*/\Gamma_{\mathrm{IIc}}$, required to satisfy the fracture criterion along the sides and front of both telephone cord and straight-sided buckles may be deduced (Fig. 18). Here, b/b_0 refers to the telephone cord (see Fig. 15), while b is the half-width of the straight-sided buckle. The mode mix, ψ, associated with the curved front of the straight-sided buckle is obtained from Fig. 10b, upon using G_{ss}/G_0 from (7). A detailed numerical analysis (Jensen and Sheinman, 2002) has established the accuracy of this approximation.

The curved front of the straight-sided configuration propagates at $G_0^*/\Gamma_{\mathrm{IIc}} \cong 0.6$, essentially independent of the width, provided that $b/b_0 > 1.5$. Stable straight-sided
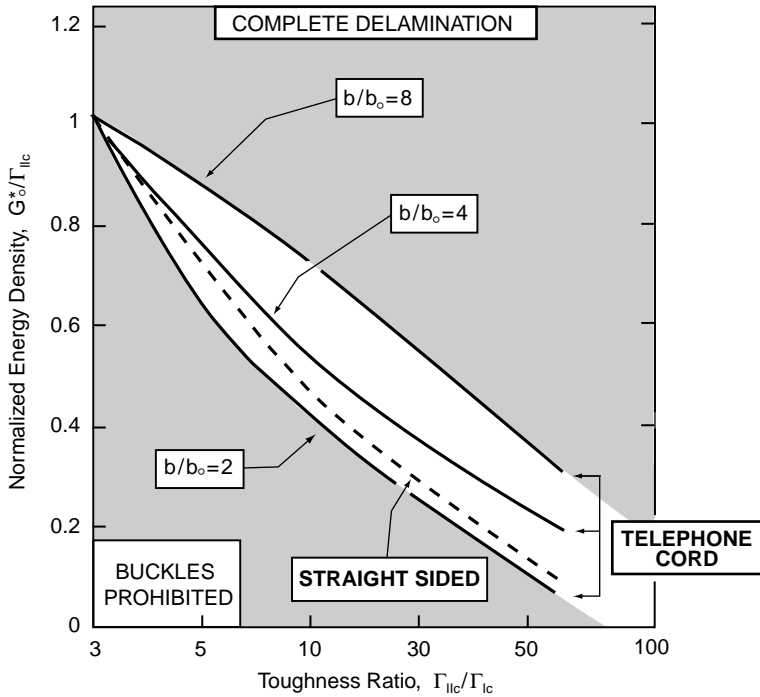
Fig. 19. Regime map for existence of the two morphologies. The mode dependence of the interface is characterized by Γ_{IIc}/Γ_{Ic} while the normalized energy/area in the film is G_0^*/Γ_{IIc}. Straight-sided buckles exist in a narrow band centered on the curve shown with $b/b_0 \cong 2$. Telephone cords exist in a relatively wide domain, with a width-dependence on G_0^*/Γ_{IIc}.

buckles would not be possible when $G_0^*/\Gamma_{IIc} > 0.6$ since the front would propagate dynamically. Two other results are consistent with this finding. (i) Straight sides become unstable to sinusoidal shape perturbations when b/b_0 exceeds a critical value (Jensen, 1993). For the present interface fracture criterion (16), this occurs at $b/b_0 \approx 2$ if $\lambda < 0.3$. (ii) The straight-sided configuration undergoes a secondary bifurcation that promotes side undulations at $b/b_0 \approx 2.5$ (Audoly, 1999; Jensen and Sheinman, 2001). *In summary, the combined results suggest that straight-sided buckles can only be expected in a narrow range of G_0^*, when $b/b_0 \approx 2$, consistent with their rarity.*

    The range of G_0^* wherein the telephone cord morphology can exist is distinctly greater. A domain map is plotted in Fig. 19 in dimensional space G_0^*/Γ_{IIc} versus $\Gamma_{IIc}/\Gamma_{Ic} = 1 + \tan^2((1-\lambda)\pi/2)$. Telephone cords cannot form below the lowest curve, $b/b_0 \cong 2$. Conversely, at large G_0^*/Γ_{IIc} the entire interface delaminates (the upper limit has not been determined, but is unlikely to be much larger than that for $b/b_0 = 8$). Straight-sided buckles are only preferred within a narrow domain near the dotted curve. Their half-width is $b/b_0 \cong 2$ for all Γ_{IIc}/Γ_{Ic}.

7. Summary

Telephone cord buckles that form beneath a highly compressed DLC film on a glass substrate have been analyzed. Profiles have been measured by AFM along radial and median trajectories. These suggest that each unit segment might be modeled as a segment of a circular buckle pinned at its center. The mechanics of this model have been presented. The results reveal that the telephone cord topology can be effectively modeled as a series of pinned circular buckles along its length, with an unpinned circular buckle at its front.

To calibrate the system, the FIB has been used to create short, straight-sided buckles from unit segments of the telephone cord and the new profiles measured by AFM. By fitting these profiles to well-established mechanics solutions, the residual compression in the DLC has been ascertained as 1.6 GPa. This stress is used with the pinned, circular buckle solutions to compare measured and predicted profiles. The close coincidence validates the model and allows energy release rates and mode mixities to be determined for the telephone cord.

The theoretical findings are consistent with the observation that telephone cords are observed in many systems, while straight sided buckles are rare.

Acknowledgements

References

Audoly, B., 1999. Stability of straight delamination blisters. Phys. Rev. Lett. 83 (20), 4124–4127.

Audoly, B., 2000. Mode-dependent toughness and the delamination of compressed thin films. J. Mech. Phys. Solids 48 (11), 2315–2332.

Chai, H., 1998. The post-buckling response of a bi-lateral constrained column. J. Mech. Phys. Solids 46 (7), 1155–1181.

Cho, S.-J., Lee, K.-R., Eun, K.Y., Hahn, J.H., Ko, D.-H., 1999. Determination of elastic modulus and poisson's ratio of diamond-like carbon films. Thin Solid Films 341, 207–210.

Colin, J., Cleymand, F., Coupeau, C., Grilhe, J., 2000. Worm-like delamination patterns of thin stainless steel films on polycarbonate substrates. Philos. Mag. A 80 (11), 2559–2565.

Evans, A.G., Hutchinson, J.W., 1984. On the mechanics of delamination and spalling in compressed films. Int. J. Solids Struct. 20 (5), 455–466.

Evans, A.G., Ruhle, M., Dalgleish, B.J., Charalambides, P.G., 1990. The fracture energy of bimaterial interfaces. Mater. Sci. Eng. A 126, 53–64.

Evans, A.G., He, M.Y., Hutchinson, J.W., 1997. Effect of interface undulations on the thermal fatigue of thin films and scales on metal substrates. Acta Mater. 45 (9), 3543–3554.

Gille, G., Rau, B., 1984. Buckling instability and adhesion of carbon layers. Thin Solids Films 120, 109–121.

He, M.Y., Hutchinson, J.W., 1989a. Kinking of a crack out of an interface. J. Appl. Mech. 56, 270–278.

He, M.Y., Hutchinson, J.W., 1989b. Crack deflection at an interface between dissimilar elastic materials. Int. J. Solids Struct. 25 (9), 1053–1067.

He, M.-Y., Bartlett, A., Evans, A.G., Hutchinson, J.W., 1991. Kinking of a crack out of an interface: role of in-plane stress J. Amer. Ceramic Soc. 74 (4), 767–771.

Hutchinson, J.W., 2001. Delamination of compressed films on curved substrates. J. Mech. Phys. Solids 49 (9), 1847–1864.

Hutchinson, J.W., Suo, Z., 1992. Mixed mode cracking in layered materials. Adv. Appl. Mech. 29, 63–191.

Hutchinson, J.W., Thouless, M.D., Liniger, E.G., 1992. Growth and configurational stability of circular, buckling-driven film delaminations. Acta Metall. Mater. 40 (2), 295–308.

Hutchinson, J.W., He, M.Y., Evans, A.G., 2000. The influence of imperfections on the nucleation and propagation of buckling driven delaminations. J. Mech. Phys. Solids 48 (4), 709–734.

Jensen, H.M., 1993. Energy release rates and stability of straight-sided, thin film delaminations. Acta Mater. 41, 601–607.

Jensen, H.M., Sheinman, I., 2001. Straight-sided, buckling-driven delamination of thin films at high stress levels Int. J. Fract., 110, 371–385.

Jensen, H.M., Sheinman, I., 2002. Numerical analysis of buckling driven delamination. Int. J. Solids Struct., in press.

Jensen, H.M., Thouless, M.D., 1995. Buckling instability of straight edge cracks. J. Appl. Mech. 62, 620–625.

Lee, K.-R., Baik, Y.-J., Eun, K.-Y., 1993. Stress relief behavior of diamond-like carbon films on glass Diamond Relat. Mater., 2.

Matuda, N., Baba, S., Kinbara, A., 1981. Internal stress, Young's modulus and adhesion energy of carbon films on glass substrates. Thin Solid Films 81, 301–305.

Moon, M.W., Chung, J.-W., Lee, K.-R., Oh, K.H., Wang, R., Evans, A.G., 2002. An experimental study of the influence of imperfections on the buckling of compressed thin films. Acta Mater. 50, 1219–1227.

Suo, Z., Hutchinson, J.W., 1990. Interface crack between two elastic layers. Int. J. Fract. 43, 1–18.

Thouless, M.D., Hutchinson, J.W., Liniger, E.G., 1992. Plane-strain, buckling-driven delamination of thin films: model experiments and mode-II fracture Acta Metall. Mater. 40 (6), 2639–2649.

Weiderhorn, S.M., 1967. Influence of water vapor on crack propagation in soda-lime glass. J. Amer. Ceramic Soc. 50 (8), 407–414.